Supporting Information

Stabilizing Oxygen-Deficient Mn Sites Active in Seawater Oxidation

Tanveer ul Haq [a]*, Mourad Smari [b], Aleena Tahir [c], and Yousef Haik [d,e]*

[a] Department of Chemistry, College of Sciences, University of Sharjah, P.O. Box, 27272 Sharjah, UAE

[b] Center for Advanced Materials Research, Research Institute of Sciences and Engineering, University of Sharjah, P. O. Box 27272, Sharjah, United Arab Emirates.

[c] Department of Chemistry & Chemical Engineering, SBA School of Science & Engineering, Lahore University of Management Sciences (LUMS), DHA, Lahore, Pakistan

[d] Department of Mechanical and Nuclear Engineering, College of Engineering, University of Sharjah, P.O. Box, 27272 Sharjah, UAE

[e] Department of Mechanical Engineering, The University of Jordan, Amman-Jordan

Corresponding Emails:

yhaik@sharjah.ac.ae

thaq@sharjah.ac.ae

Materials

Ni Foam (0.25 mm, Sigma Aldrich), Calcium nitrate hydrate, ($Ca(NO_3)_2 \cdot 4H_2O$, 99%, Sigma Aldrich), Manganese chloride hydrate ($MnCl_2 \cdot 4H_2O$ 99% Sigma Aldrich), Potassium per manganate ($KMnO_4$, 99.0 %), Sigma Aldrich), Iridium oxide (IrO_2, 99%, Sigma Aldrich), Pt/C (Sigma Aldrich), Sodium chloride (NaCl, Sigma Aldrich), Sulfuric acid ($H_2SO_4 \geq 98\%$, Sigma Aldrich), Potassium hydroxide (KOH, $\geq$95%, Sigma-Aldrich), Sodium hydroxide (NaOH, $\geq$95%, Sigma-Aldrich), Hydrochloric acid (HCl, 37 %, Alfa Aesar), Ethanol (C2H5OH, $\geq$ 98%, Sigma Aldrich), Methanol (CH3OH, $\geq$ 98%, Sigma Aldrich), Isopropanol ($\geq$ 98%, Sigma Aldrich). Milli-Q ultrapure water with resistance of 18 M Ω cm-1 was used throughout this study.

Synthesis of MnO_x and $CaMnO_x$

MnOx nanorods were synthesized through hydrothermal techniques. To prepare the required solutions, 0.05 M $KMnO_4$ and 0.2 M $MnCl_2 \cdot 4H_2O$ were dissolved in deionized water. The synthesis process involved gradually combining 30 mL of $KMnO_4$ solution with 30 mL of $MnCl_2 \cdot 4H_2O$ solution. The addition of hydrochloric acid (HCl) adjusted the pH to 2, and the resulting solution was further diluted with deionized water to a total volume of 75 ml. This solution was then placed in a Teflon Lined Hydrothermal Autoclave (150 mL) for hydrothermal treatment at 180 °C for 18 hours, promoting the formation and growth of MnOx nanorods.

Similarly, CaMnOx nanorods were fabricated using the same synthesis approach. Solutions of 0.05 M $KMnO_4$, 0.2 M $MnCl_2 \cdot 4H_2O$, and 0.25 M $Ca(NO_3)2 \cdot 4H_2O$ were prepared with deionized water. In the synthesis process, 20 mL of $KMnO_4$ solution and 20 mL of $Ca(NO_3)2 \cdot 4H_2O$ solution were combined, and subsequent additions of KOH were made until the pH reached 14. After cooling to room temperature, 20 mL of $MnCl_2 \cdot 4H_2O$ solution was added dropwise. The resulting solution was diluted with deionized water to a total volume of 75 mL and transferred to a Teflon Lined Hydrothermal Autoclave (150 mL) for hydrothermal treatment at 180 °C for 18 hours, facilitating the formation and growth of CaMnOx nanorods. Both samples underwent thorough washing with deionized water and ethanol and were subsequently dried in an oven at 65 °C for 12 hours.

Structural and Chemical Characterization

The crystal phase of all prepared materials was determined using a Bruker D8 Advance diffractometer with Cu Kα radiation (λ = 1.54056 Å) as the X-ray source in the 2θ range of 05–

90°. Scanning Electron Microscopy (SEM) analysis, conducted with a Thermo Fischer NOVA Nano SEM 450-FEISEM and Energy Dispersive Spectrometer (Oxford Instruments, UK), was employed to investigate the surface structure and composition of the materials. Raman spectra were obtained using an InVia Raman Microscope-Renishaw with a wavelength of 514 nm. X-ray Photoelectron Spectroscopy (XPS) studies were performed using a Kratos X-ray Photoelectron Spectrometer–Axis Ultra DLD with an Al mono (K-alpha) source operated at 15 keV and 15 mA to study the chemical structure of the materials.

Electrochemical Characterizations

Electrochemical measurements of these as-prepared catalysts were performed on a Gamry Reference 3000 electrochemical station using a three-electrode setup. The as prepared catalyst, Hg/HgO and graphite rode were used as working, reference, and counter electrodes, respectively. The cyclic polarization curve of each catalyst was conducted at low scan rate (1 mV/s) with 10 % iR compensation. Initially 20 cycles were performed for each catalyst to stabilize the active sites. All the potentials were calibrated to the reversible hydrogen electrode using the equation: E RHE = E Hg/HgO + 0.098 V + 0.059 PH. The Tafel slope was determined by $\eta = a + b \log (j)$, where j represents the current density. The electrochemical impedance spectroscopy (EIS) calculations were completed under similar conditions at an overpotential near to-onset potential from 10^6 to 10^{-1} Hz with an A.C voltage of 5 mV/s.

Electrochemical active surface area (ECSA)

The electrochemically active surface area was calculated following a standard formula: ECSA $=R_f*S$, where S denotes the real surface area of the smooth electrode, equivalent to the geometric area of the working electrode (in our case S= 1cm^2).[1]

$$ECSA = R_f S$$

The roughness factor (R$_f$) was determined using the following equation.

$$R_f = \frac{C_{dl}}{C_s}$$

Here, C$_{dl}$ represents the double-layer capacitance, obtained from the slope of the double-layer charging current versus the scan rate using the equation.

$$i_c = vC_{dl}$$

where Cs is the specific capacitance of a sample under the specific condition of electrolyte and C_{dl} is the double-layer capacitance in the non-faradic region of the voltammogram. C_s, denoting the general specific capacitance, represents the average double-layer capacitance of a smooth material surface, typically ranging from 20 to 40 μFcm^{-2} Hence, we chose an average value (0.040 mF) to get the average value of ECSA of our catalyst.

Exchange current density from EIS

Exchange current density $(I_{ex}) = \dfrac{RT}{nF\theta}$

R = Gas constant (8.314 j/ K. mol)

T = Reaction temperature

n = Number of electrons transfer (4)

θ = Charge transfer resistance calculated from the EIS.

CaMnO$_x$-Ni(OH)$_2$

$$\frac{8.314 \text{ J/K. mol} * 298 \text{ K}}{4 * 96485 \text{ Cmol}^{-1} * 8.0 \ \Omega * 1 \text{ cm}^2}$$

$$= 0.79 \text{ mA/cm}^2$$

MnO$_x$-Ni(OH)$_2$

$$\frac{8.314 \text{ J/K. mol} * 298 \text{ K}}{4 * 96485 \text{ Cmol}^{-1} * 16.1 \ \Omega * 1 \text{ cm}^2}$$

$$= 0.22/\text{cm}^2$$

Ni(OH)$_2$

$$\frac{8.314 \text{ J/K. mol} * 298 \text{ K}}{4 * 96485 \text{ Cmol}^{-1} * 24.9 \ \Omega * 1 \text{ cm}^2}$$

$$= 0.12 \text{ mAcm}^2$$

Determination of TOF from the integrated OER polarization curve

$$TOF = \frac{i \times N_A}{A \times F \times n \times r}$$

Were,

i = current in Ampere

N_A= Avogadro number

A = Geometrical surface area of the electrode

F = Faraday constant

n = Number of electrons

r = Surface concentration of atoms

TOF of synthesized catalyst for OER

OER @1.6 V vs RHE

$CaMnO_x$-Ni(OH)$_2$ $= \dfrac{0.5A \times 6.022 \times 10^{23}\ atom}{1cm^2 \times 96485C \times 4 * 4.9 \times 10^{15} atoms}$

$= 160\ \text{s}^{-1}$

MnO_x-Ni(OH)$_2$ $= \dfrac{0.3A \times 6.022 \times 10^{23}\ atom}{1cm^2 \times 96485C \times 4 * 5.2 \times 10^{15} atoms}$

$= 90\ \text{s}^{-1}$

Ni(OH)$_2$ $= \dfrac{0.15A \times 6.022 \times 10^{23}\ atom}{1cm^2 \times 96485C \times 4 * 7.3 \times 10^{15} atoms}$

$= 32\ \text{s}^{-1}$

Faradic efficiency

The water displacement method was used for the quantification of molecular O_2. The ideal gas equation was used for the quantitative analysis, where we assumed that all the electrons in the external circuit are generated during OER process which can later reduce the protons. In this set-up, electrochemical airtight cell was connected with the graduated burette filled with water. Initially, the cell was purged with nitrogen for 15 minutes followed by chronopotentiometry experiments, while noting the initial volume. The reduction in the water volume was observed

directly linked with increase in the volume of gas in the head space of the burette. The measured volume was then converted into faradic efficiency by comparing with theoretical yield using the formula.

Faradaic efficiency = $V_{experimental}$ / $V_{Theoretical}$

While

$V_{Theoretical\ for\ O2}$ = $1/4 * Q/F * V_m$

The number 1 means 1 mole of O_2 per mole of H_2O and 4 means 4 moles of electrons per mole of H_2O.

$V_{Theoretical\ for\ H2}$ = $1/2 * Q/F * V_m$

The number 1 means 1 mole of O_2 per mole of H_2O and 2 means 2 moles of electrons per mole of H_2O.

Q= It (amount of charged passed through electrode)
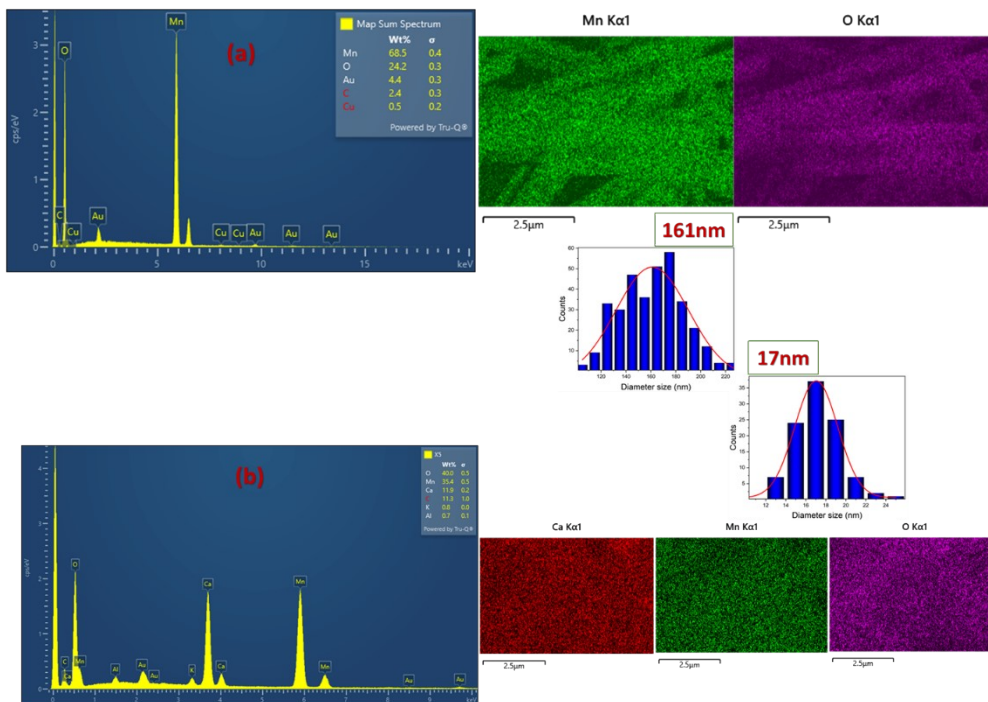
F = Faraday constant (96485 C mol^{-1})

Figure S1. (a) EDX spectrum and nanorods distribution of (a) MnO_x and (b) $CaMnO_x$ nanorods
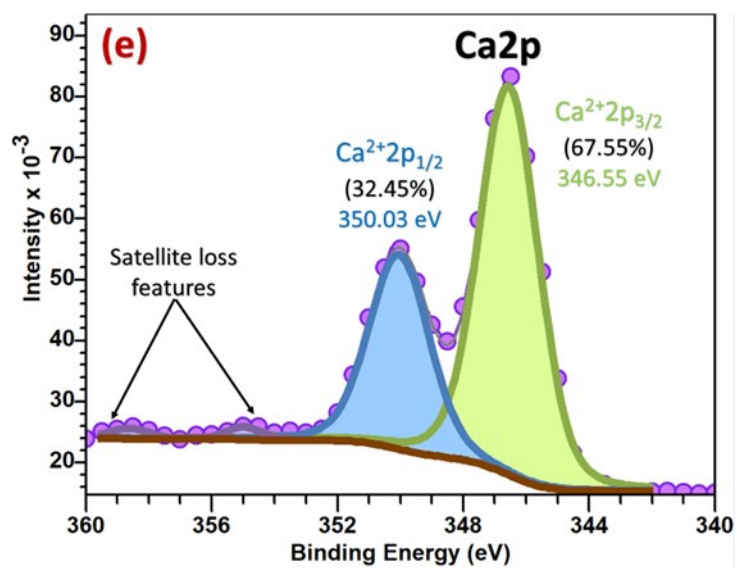
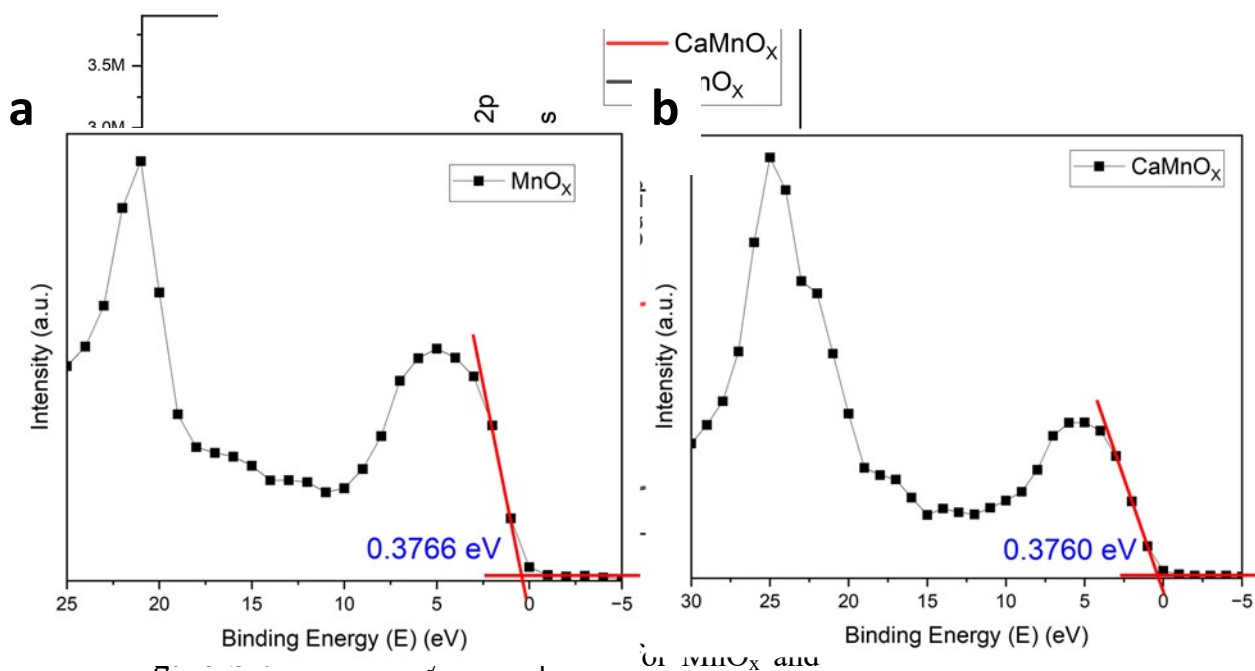**Figure S3.** High resolution XPS spectrum of Ca2p for CaMnOx nanorods

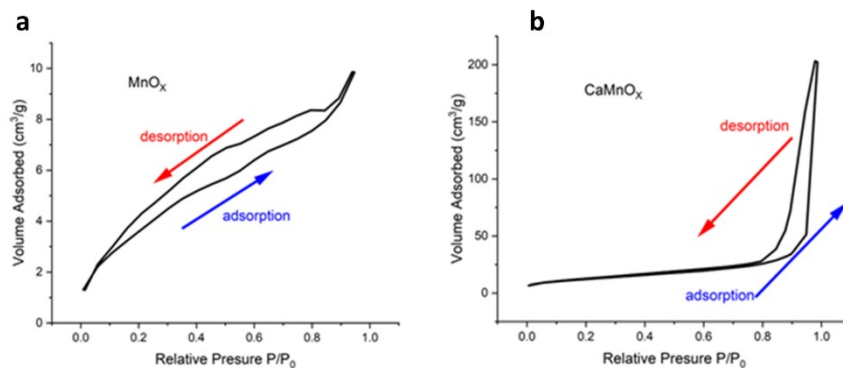**Figure S4**. Valence band spectra MnO_x and $CaMnO_x$ nanorods.

Figure S5. BET analysis of MnO$_x$ and CaMnO$_x$

BET analysis of CaMnO$_x$

Weight=0.0322 g
Description Analysis
Molecular Weight   28.0134 g
Cross Section Area   16.2 Å²/molec
Bath Temperature   77.35 K
Isotherm Branch   Adsorption

Slope   79.8819
Intercept   0.600856
Correlation coeff., r   0.999727
C constant   133.947
Surface area   43.270 m²/g

Table - BET Multi-point BET.

Relative Pressure	Volume Adsorbed cc/g	1 / [W((P/Po) - 1)] @STP
0.05494	9.12667	5.0967
0.10757	10.3364	9.3304
0.11767	10.5808	10.0847
0.15739	11.3633	13.1521
0.20375	12.2413	16.725
0.22762	12.6962	18.5717
0.2548	13.2407	20.6621
0.30338	14.0762	24.7549
0.33578	14.7048	27.506
0.35452	15.0144	29.2683

BET analysis of MnO$_x$

Weight 0.0331 g
Description Analysis
Molecular Weight 28.013g
Cross Section Area 16.2 Å²/mol
Bath Temperature 77.35 K
Isotherm Branch   Adsorption

Slope 222.738
Intercept 10.5694
Correlation coeff., r 0.999481
C constant 22.0737
Surface area 14.927 m²/g

Table - BET Multi-point BET.

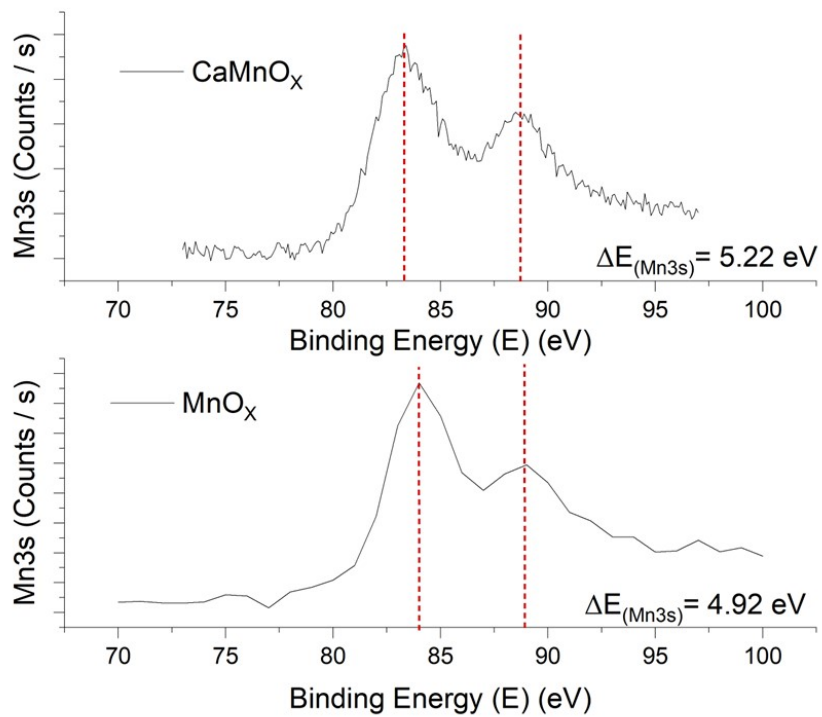| Relative Pressure	Volume Adsorbed cc/g	1 / [W((P/Po) - 1)] @STP
0.05838	2.21627	22.3821
0.10813	2.75687	35.1855
0.15527	3.18913	46.114
0.20698	3.64969	57.2179
0.25652	4.086	67.5603
0.30423	4.50818	77.6034
0.35208	4.88435	89.014

Figure S6. Mn 3s XPS spectra of MnOx and CaMnOx nanorods
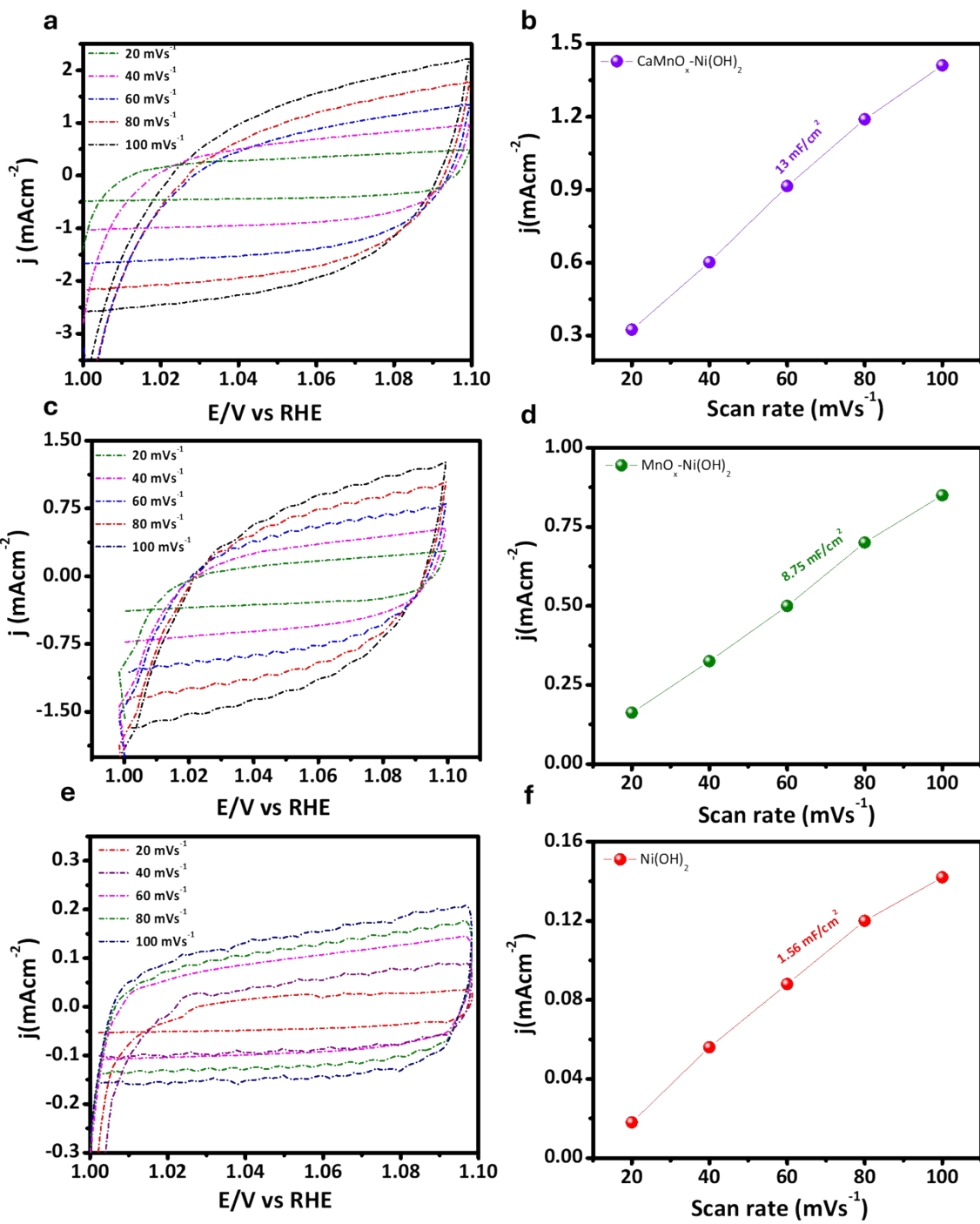
Figure S7 Static cyclic voltammetry curves at 20, 40, 60, 80 and 100 Vs^{-1} and dependence of double layer charging current vs. scan rate plots of (a,b).$CaMnO_x$-$Ni(OH)_2$, (c,d) MnO_x- $Ni(OH)_2$ and (e,f) $Ni(OH)_2$,
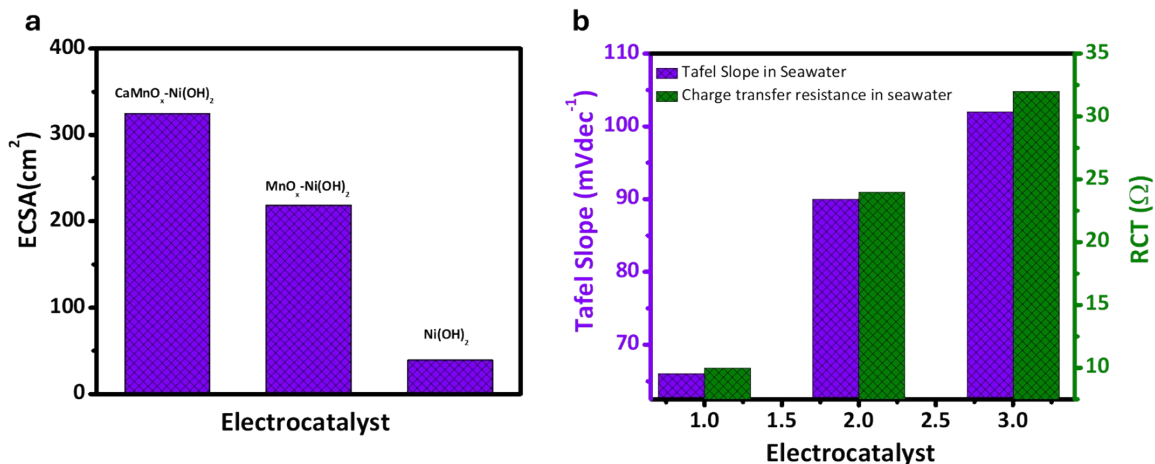
Figure S8. (a) Electrochemical active surface area, (b) Tafel slope and charge transfer resistance of $CaMnO_x$, MnO_x, $Ni(OH)_2$ in alkaline seawater
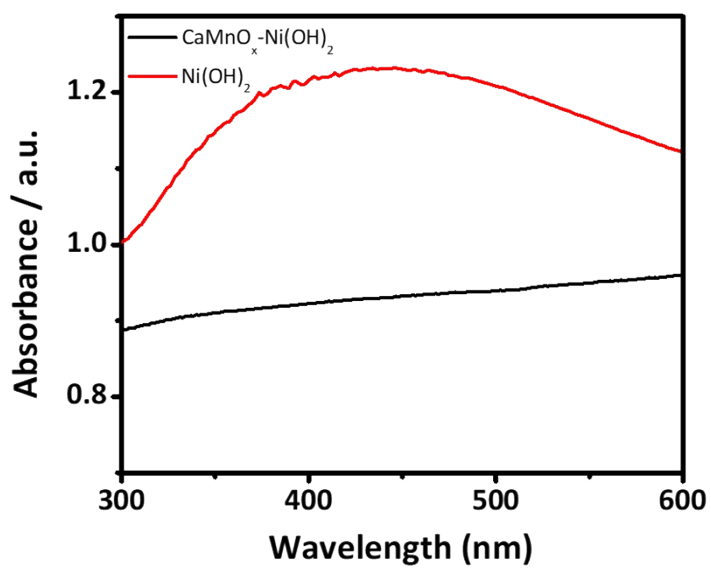

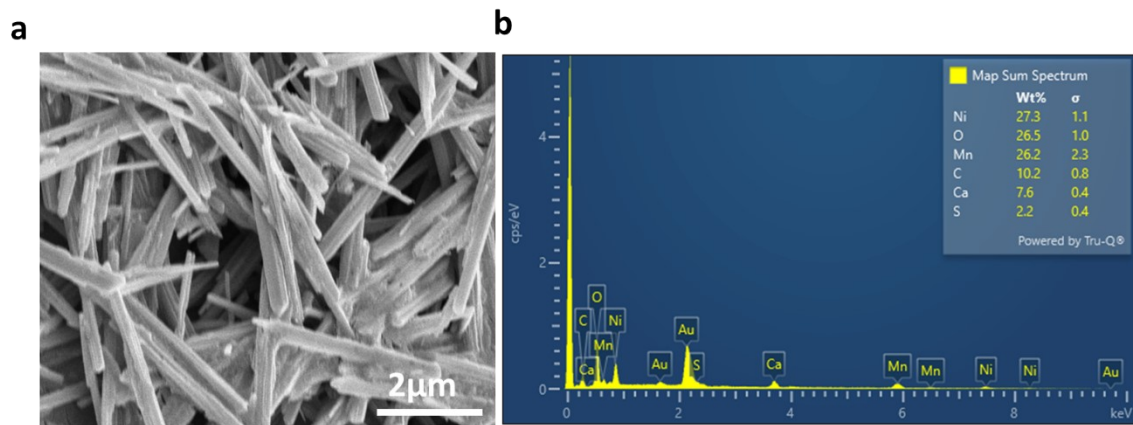**Figure S9**. (a) SEM image and (b) EDS spectrum of $CaMnO_x$-$Ni(OH)_2$ after seawater electrolysis.

Figure S9. (a) SEM image and (b) EDS spectrum of $CaMnO_x$-$Ni(OH)_2$ after seawater electrolysis.

Table S1. Quantitative analysis of MnO_x and $CaMnO_x$ nanorods

Samples	Surface Area (m2/g)	Total Pore Volume (cc/g)	Ratio Mn^{3+}/Mn^{4+}	Ratio O_{ads}/O_{latt}	AOS	VB-XPS
MnO_x	14.927	0.01257	0.09	0.425	3.416	0.3766
$CaMnO_x$	43.270	0.3138	0.41	1.254	3.078	0.3760

Table S2. Comparison of the OER activity between CaMnO$_x$-Ni(OH)$_2$ and other previously reported catalysts in alkaline and alkaline sea water electrolytes.

Electrocatalyst	η@10mAcm^{-2} (mV)	Tafel slope (mVdec^{-1})	Electrolyte	References
CaMnO$_x$-Ni(OH)$_2$	260	63	1M KOH	This Work
Ni-CO@NC (N-doped carbon nanofiber)	530	98	1 M KOH	[2]
Ni/ Ni (OH)$_2$	403	74.8	1M KOH	[3]
K1-xNax(MgMnFeCoNi)F3	300	55	1M KOH	[4]
CaMnO$_x$-Ni(OH)$_2$	280	65	1M KOH Seawater	This Work
Ni-Mo-N @NiFeN	286	58.6	1M KOH seawater	[5]
B-Co$_2$Fe LDH	245	63.8	1M KOH seawater	[6]
Ni$_2$P/Fe$_2$P/NF	220	86	1M KOH seawater	[7]
Co-Fe$_2$P	250	45	1M KOH seawater	[8]
Na$_2$Co$_{1-x}$Fe$_x$P$_2$O$_7$	280	53	1M KOH+0.5M NaCl	[9]

References

1   C. C. L. McCrory, S. Jung, J. C. Peters and T. F. Jaramillo, *J. Am. Chem. Soc.*, 2013, **135**, 16977–16987.

2   Y. Fu, H. Y. Yu, C. Jiang, T. H. Zhang, R. Zhan, X. Li, J. F. Li, J. H. Tian and R. Yang, *Adv. Funct. Mater.*, , DOI:10.1002/adfm.201705094.

3   D. Lim, S. Kim, N. Kim, E. Oh, S. E. Shim and S. H. Baeck, *ACS Sustain. Chem. Eng.*, 2020, **8**, 4431–4439.

4   T. Wang, H. Chen, Z. Yang, J. Liang and S. Dai, *J. Am. Chem. Soc.*, 2020, **142**, 4550–4554.

5   L. Yu, Q. Zhu, S. Song, B. McElhenny, D. Wang, C. Wu, Z. Qin, J. Bao, Y. Yu, S. Chen and Z. Ren, *Nat. Commun.*, 2019, **10**, 1–10.

6   L. Wu, L. Yu, Q. Zhu, B. McElhenny, F. Zhang, C. Wu, X. Xing, J. Bao, S. Chen and Z. Ren, *Nano Energy*, 2021, **83**, 105838.

7   L. Wu, L. Yu, F. Zhang, B. McElhenny, D. Luo, A. Karim, S. Chen and Z. Ren, *Adv. Funct. Mater.*, 2021, **31**, 1–12.

8   S. Wang, P. Yang, X. Sun, H. Xing, J. Hu, P. Chen, Z. Cui, W. Zhu and Z. Ma, *Appl. Catal. B Environ.*, 2021, **297**, 120386.

9   H. J. Song, H. Yoon, B. Ju, D. Y. Lee and D. W. Kim, *ACS Catal.*, , DOI:10.1021/acscatal.9b04231.